Submitted to ADVANCED OPTICAL MATERIALS

DOI: 10.1002/adom.((please add manuscript number))
Article type: Full Paper

Plasmonic Gas Sensing using Nanocube Patch Antennas

Alexander W. Powell, David M. Coles, Robert A. Taylor, Andrew A.R. Watt, Hazel E. Assender and Jason M. Smith*

A. W. Powell, Dr. D. M. Coles, Prof. A. A. R. Watt, Prof. H. E. Assender, Prof. J. M. Smith
Dept. Materials, University of Oxford, Parks Road, Oxford, OX1 3PQ, UK
E-mail: alexander.powell@materials.ox.ac.uk

Prof. R. A. Taylor
Dept. Physics, University of Oxford, Parks Road, Oxford, OX1 3PU, UK

Keywords: plasmon; sensor; gas; humidity; nanocube;

We demonstrate the utility of individual nanocube patch antennas, consisting of a silver nanocube separated from an Ag sheet by a thin fluoropolymer spacer, to act as subwavelength sensing elements. An increase in relative humidity (RH) causes the spacer to expand, which alters the resonance of the plasmon cavity mode formed between the cube and the sheet. Using bottom-up fabrication techniques, sensitivities up to 0.57 nm/% RH are recorded, and a resolution of better than 1 % RH achieved with a rapid response time, making this the most effective single nanoparticle plasmonic humidity sensor to date. Finite-difference time-domain simulations are conducted to understand the effects of particle geometry on the sensitivity. This platform could be utilised to detect a variety of gases with an appropriate choice of spacer material, and could be scaled up to create a large-area metamaterial sensor, or used as a subwavelength sensing element with the potential for integration into plasmonic circuitry.

1. Introduction

Over the last decade there has been a concerted effort to develop plasmon-based or enhanced sensors[1–3] to follow up on the great success story of surface enhanced Raman spectroscopy.[4] Localized surface plasmons (LSP's) are attractive for sensing as they offer orders of magnitude electric field enhancements which are extremely sensitive to the immediate dielectric environment.[5-9] Plasmonic sensing offers a number of advantages compared to conventional electrochemical methods, with faster response times,[5,6] the potential for increased sensitivity[7–9] and low susceptibility to external electromagnetic (EM) radiation. With length scales below the diffraction limit, and fast operational speeds, well-designed plasmonic sensors also have potential for integration with on-chip photonic or plasmonic circuits.[10,11]

To utilise a plasmonic sensor across a range of applications, the plasmon resonances must be tunable to the spectral region of interest and be as sensitive as possible to small changes in the local environment. Whilst individual particle resonances can be effectively tuned through size, shape and material choice,[2,12] coupled modes between two or more nanoparticles have been shown to exhibit far greater electric field enhancements and produce more sensitive detectors.[13–1516–18] However, these are extremely difficult to fabricate, with many top-down lithographic and FIB based examples being unrealistic for scaling up, and bottom-up techniques that generally produce randomly oriented particle pairs with no control over the alignment, which is key as the resonances of such dimers are highly sensitive to the polarisation of incident illumination. Henzie et al. made some important progress in this field by using a gravity-driven technique to assemble nanoparticles in shallow pits in a substrate,

which allows excellent control over orientation and positioning of any number of particle sets.[19] Another elegant solution to the fabrication problem is the placement of a metallic particle above a metal sheet separated by a thin spacer. A 'mirror particle' is excited in the metal plane which produces a strong coupling effect without having to align two separate particles, drastically simplifying the production process.[20-20] There is a growing body of work investigating the properties of silver nanocubes (NC's) above metal films, to tune their scattering properties,[21] produce controlled-reflectance surfaces,[22] and to control and enhance the radiative processes of fluorophores within the spacer material,[23,24] as well as theoretical studies looking to build a complete description of the structure.[25,26]

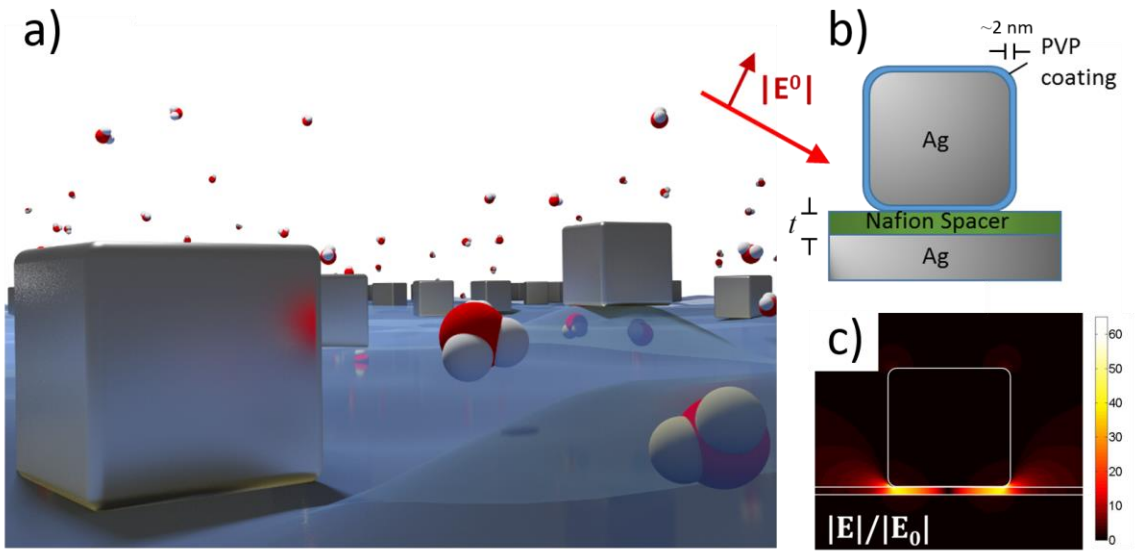

Figure 1. (a) Artistic image showing the nanocubes resting on a Nafion film interacting with water molecules (b) The basic setup for simulations and experiments in this report: a silver NC with a PVP coating is separated from a silver film by a Nafion spacer layer. It is illuminated and the scattered light used to characterise the system. (c) FDTD simulation showing the (normalized) electric field intensity of the principal mode excited between a NC and an Ag sheet with a 5 nm spacer.

This system can be considered an optical patch antenna, where gap plasmon modes are supported between the metal sheet and the NC.[21] The resonant modes of these antennae are extremely sensitive to the properties of the spacer layer separating the NC and the silver sheet, and any environmental changes that influence the refractive index (RI), or more importantly the thickness of the chosen material will produce significant changes in the plasmon resonance. As long as spacer materials which expand in response to a given analyte are available, this design can be utilised to detect any number of chemicals. This forms the basis for a new type of sensor, which can operate equally well in a gaseous or liquid setting (depending on spacer choice) and that is scalable from the sub-wavelength scale (the footprint of one nanocube) up to a large-surface area metamaterial.

In this paper we demonstrate the operation of the nanocube patch antenna system as a gas sensor for the first time, using the Nafion fluoropolymer from Dupont as our spacer material. Nafion is a Poly(perfluorosulfonic acid)-based ion-conducting membrane with a hydrophobic fluorocarbon polymer backbone and hydrophilic sulfonic acid side chains which allow it to take on water from its surroundings and expand significantly with increasing humidity[27–29] (See figure S1 for the chemical structure of Nafion). We demonstrate the tunability of the principal waveguide mode using basic fabrication techniques, and the use of this system as a humidity sensor, both through measuring resonance shifts and variations in the scattering intensity from illumination by a red laser. A road to enhancing the sensitivity is also explored using Finite-difference time-domain (FDTD) simulations and the potential for integration of this design with a photonic waveguide is discussed.

2. Experimental Results

Figure 1 displays the geometry of a film-coupled nanocube antenna sensing element. Figure 1(a) is an artistic impression of the silver NC's resting on the Nafion spacer layer above the silver film, with H_2O molecules in the local environment and some being absorbed into the Nafion spacer leading to local swelling. The basic geometry used for simulations and experiments in this report is shown in Figure 1(b). Figure 1(c) shows the electric field intensity distribution of the fundamental cavity mode beneath a 75 nm cube with 10 nm RoC edges, calculated using finite difference time domain modelling. It can be clearly seen that the electric field is concentrated between the NC and the metal film, inside the Nafion spacer, with the strongest concentration near the corners. This field concentration is the origin of the extreme sensitivity to changes in the spacer layer.

The mode shown in figure 1(c) is formed from coupled plasmon oscillations across the near face of the cube and the surface of the metal sheet, which possess mirrored charge separations, producing a very concentrated electric field. This can be considered as an optical patch antenna formed by the flat face of the cube on top and the metal sheet below.[21,30,31] Reflections at the cube edges lead to resonances, and the wavelength of the fundamental resonance, λ_{pk}, for a cube with perfectly sharp corners, corresponds to a half wavelength in the cavity and is related to the cube width, w by: $\lambda_{pk} = 2n_{eff}w$ where n_{eff} is the effective index of the mode inside the spacer. The linear relationship between w and λ_{pk} has been demonstrated experimentally.[21]

Through considering the lossy nature of the surface plasmons, Bozhevolnyi *et al.* demonstrated that the relationship between n_{eff} and the spacer thickness, t can be said to be inversely proportional for very thin spacers[30] so: $\lambda_{pk} \sim n_{eff}w \sim w/t$, (although the precise relationship for films thicker than a couple of nm is more involved - see supporting

information). A generally reciprocal relationship between the resonance properties and the coupling distance is to be expected for an evanescent effect such as plasmonic coupling. As the resonance is only dependent on *w* and *t*, it is extremely insensitive to polarization and angle of incidence, making arrays of these antennas extremely useful for selective reflection coatings.[21,22] It has been demonstrated that the optical properties of nanocubes are very close to those of nanorods and nanostrips,[22,32] therefore this 2D model can be used to understand the relationship between cube size, spacer properties and the resonance conditions and sensitivity of the fundamental mode, although the importance of corner geometry to NC behaviour is so far neglected; this is discussed later and also in the work of Bowen and Smith.[25]

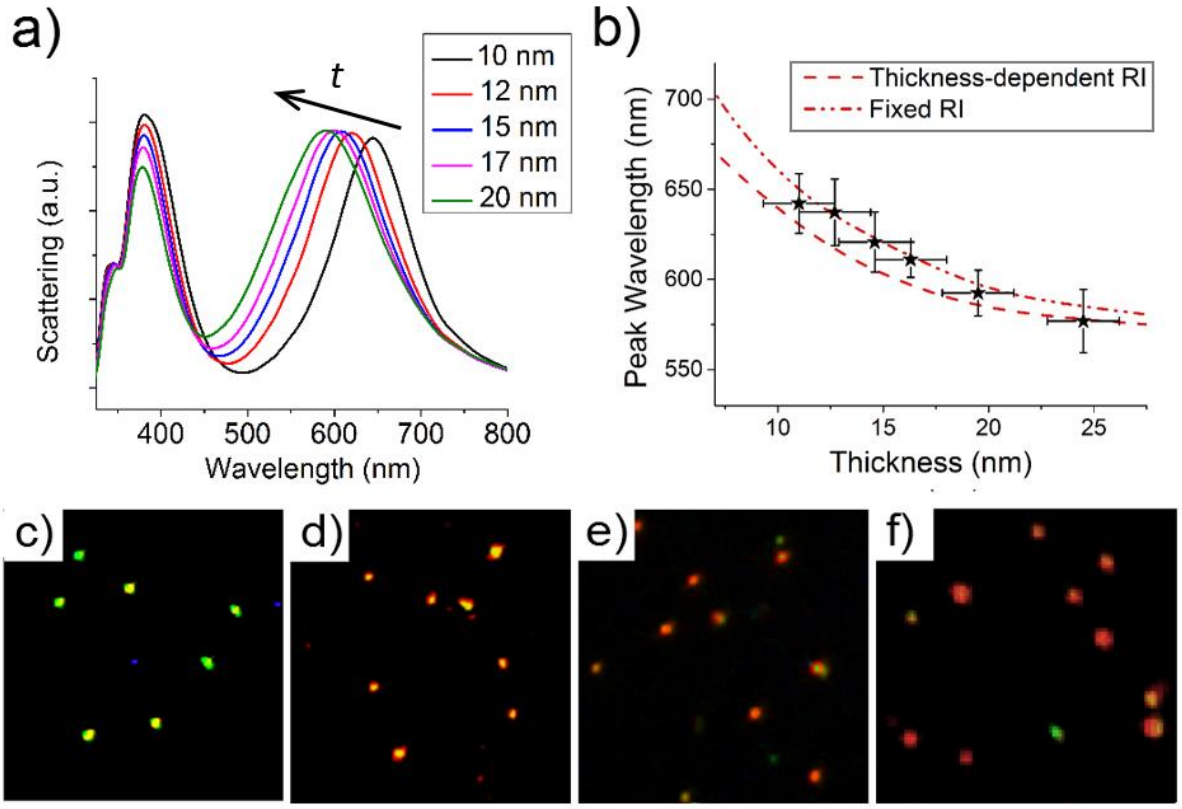

Figure 2. (a) FDTD simulation showing the wavelength shift of the principal mode as the thickness of the Nafion spacer is increased. (b) Plot showing simulated peak wavelength for a spacer RI fixed at 1.35 (dash-dot line) and one which varies with thickness (dashed line), compared to experimental dark-field scattering results (black stars) for 75 nm NC's on

varying thicknesses of Nafion polymer. (c)-(f) Dark-field CCD images of NC's above 110, 16, 13 & 11 nm Nafion films.

Figure 2(a) shows an FDTD simulation of the scattering spectra of a single NC above an Ag sheet with varying thicknesses of Nafion spacer. The fundamental mode manifests as a peak around 600 nm, which redshifts as the film thickness is decreased, due to an increase in the effective index within the cavity.[30] There are a variety of other modes which can be excited in this system,[21] which appear as shorter wavelengths peaks in the scattering spectra, but as these show a much weaker wavelength dependence on the spacer properties, they are of limited interest for this application.

Simulated values of the resonance peak positions for varying ambient spacer thicknesses, are compared with experimental results in figure 2(b). Experimental values of λ_{pk} were taken from dark-field scattering spectra from NC's above spin-coated Nafion films from 11 – 24 nm, with 50 NC's in each sample. A clear reciprocal relationship between thickness and resonance wavelength is observed, with a stronger redshifting of the peak for thinner films in line with an increasing effective index (see figure S3).

The refractive index of very thin Nafion films is known to depend upon the film thickness (figure S4), but this change is small compared to the change in effective index due to the increased density of states in the gap, as determined by the spacer thickness. A good agreement is seen between the experimental data and simulations both where the thickness-dependent RI of Nafion is considered, and where a constant RI of 1.35 is assumed. Uncertainty in the experimental data is due to the range of NC dimensions in the sample and local variations in the thickness of the Nafion layer from the spin coating, which will affect the resonance conditions of each particle. The resonance shift is significant enough that it can be detected visually, as shown by figures 2(d)-(f), where white-light scattering from 11, 13

and 16 nm samples show a clear shift from a deep red to a yellowy orange as the film thickness increases. Also shown in figure 2(c) is a sample with a 110 nm film showing a peak strongly in the green, demonstrating a resonance with negligible coupling between the cube and the metal.

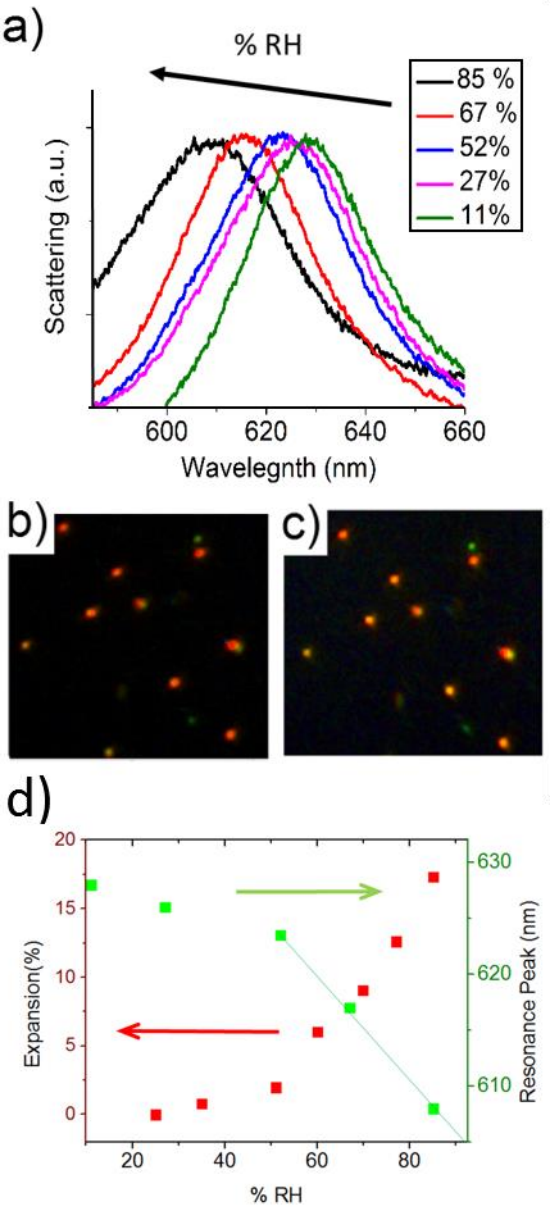

Figure 3. (a) Normalised experimental scattering spectra of a 75 nm Ag cube separated by a silver sheet by a 11 nm spacer under conditions varying from 11-85 % RH. (b),(c) Dark-field image of NC scattering under 11 % and 85 % RH respectively. (d) Resonance peak position vs RH for the NC measured in (a), compared with the % thickness increase of a bare Nafion

film measured on the ellipsometer. A fit line demonstrating the approximately linear relation between RH and peak position in the rapid swelling regime above ~50 %RH is also shown.

Agreement between simulation and experiment here demonstrates that the peak resonance is tunable through altering the thickness of the spacer layer using basic deposition techniques. As Nafion is known to expand and contract with humidity variations, we now have the basis for a sensor. The utility of the patch antenna geometry as a gas sensor is demonstrated in **figure 3**, where the samples are placed inside a humidity chamber and the RH of the enclosed environment is altered whilst scattering spectroscopy is performed. Figure 3(a) shows a marked redshifting of the peaks as the humidity increases and the spacer takes on water and expands. This process was found to be reversible and showed identical results after several repeats which is expected from previous studies of Nafion films, which found them to be highly robust giving nearly identical results after 50 days usage.[33] The resonance shift can be observed visually, and varying the RH from the lower range of our apparatus at 11 % RH, to the upper at 85 % RH, produces a noticeable shift from a deep red to a much brighter orange (figure 3(b) and (c)).

In figure 3(a) and (d) it can be seen that peak shifts are greater for larger humidities, and that there are at least two regions of differing expansive behaviour for the Nafion. This has been observed previously and the small expansions below ~50 %RH are attributed to individual domain growths which are very limited by the matrix of hydrophobic backbones. Above ~50 %RH these domains coalesce and cooperative effects of ionic groups overcome the mechanical resistance, leading to a reduced elastic modulus and greater expansions.[34] The response of the thickness of a bare Nafion film and the resonance peak wavelength to RH are shown to be closely related in figure 3(d) and in the rapid swelling regime above 50 %RH, both follow an approximately linear trend. An analysis of the relationship between RH and

resonance wavelength in the region between 52-85 % RH found a linear fit to be a good approximation, with an average R^2 coefficient of determination from 10 separate NC's of 0.98. This region is therefore chosen to investigate the relationship between film thickness and peak shift and to determine the sensitivities of the system.

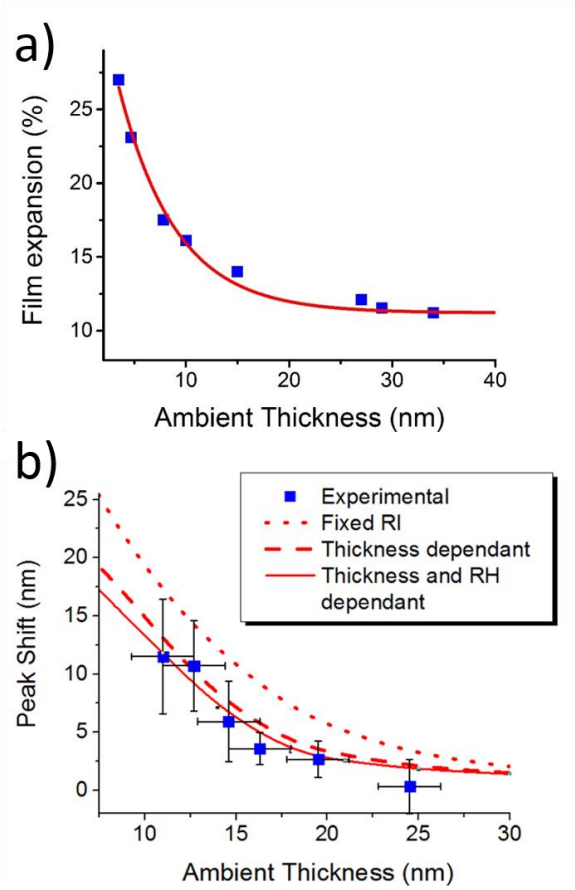

Figure 4. (a) Expansion as a percentage of ambient thickness for Nafion films as RH changes from 52-85 % as measured via ellipsometry and fitted to an exponential curve. (b) Experimental (blue squares) resonance shift for 75 nm, 10 nm RoC Ag NC's above a silver film with various spacer thicknesses, with simulated shifts based on the expansions in (a) where the RI of the films is fixed (dotted line), where it varies with thickness only (dashed line) and where it varies with thickness and RH (solid line).

Due to the inverse relationship between the mode effective index and spacer thickness, (figure S3) scattering from NC's above thinner films will show a much greater shift in resonance wavelength than thicker films for a given change in spacer thickness. Ellipsometer

measurements of the expansion of Nafion films when RH is varied from the ambient level of 52 % up to 85 % (**figure 4**(a)) show that thinner films also expand a much larger fraction of their initial width, following an approximately exponential relationship. Whilst a quantative model is lacking, it has been suggested that this behaviour is due to a reduced ability of the Nafion in very thin films to phase segregate and form the rigid backbone structures that generally exist in thicker films, which limit the water absorption capacity, leading to runaway expansion in very thin films.[35] Temperature has also been shown to be a factor in the RH response of Nafion,[36] and is discussed further in the supporting information.

We therefore expect to see the much greater shifts for a given RH change in thinner films shown in figure 4(b). Experimental data are plotted here against values from FDTD simulations taking the expansion fraction from the fit line in figure 4(a). When the RI dependence on film thickness (shown in Fig. S4(a)) is taken into account, the reduction of the Nafion RI with film thickness results in a decrease in the gradient of the fit, and the data and simulations demonstrate good agreement. Some variation of the film's RI is found with the absorption of water, although since the RI of dry Nafion is similar to that of water this is found to be small (around a 1% variation), as shown in figure S4. When the RI shift of the expanding Nafion is also included, the fit is slightly improved, although both cases agree well within error, once again showing that shifts in the RI of Nafion due to structural changes are less significant compared with the dependence of n_{eff} on spacer thickness, but must be taken into account to obtain a good fit. The good match between theory and experiment also indicates that the presence of the NC's above the film does not significantly affect water uptake.

There are significant sources of uncertainty in the results, especially for thinner layers, again due to lack of monodispersity in the cubes, surface roughness and the fact that any

inhomogeneities in the ambient film will be accentuated through uneven expansion.[37] However, the trend is very much in line with the predictions of the leaky cavity model and our knowledge of Nafion expansion. Therefore the best sensors must use the thinnest films available where the expansion properties can be maintained.

The best average humidity sensitivity of this system over the range considered is found to be 0.37 nm/% RH for NC's above an 11 nm film, with an average FWHM of 47 nm. Certain individual NC's show much higher sensitivities, of up to 0.57 nm/% RH, which is probably due to the individual NC's having sharper corners as will be discussed in the next section. This result is an improvement on previous systems based around plasmonic resonance shifts due to changing polymer refractive index around single NP's, the best of which, by Wang et al, produced a sensitivity of ~0.19 nm/% RH.[6] This result in itself is an order of magnitude improvement on previous work using bare nanoparticles.[38] Following the fit line in figure 4, we can predict that sensitivities of around 0.66 nm/% RH should be achievable for the same cubes on thinner Nafion films, with even greater enhancements possible using larger NC's with sharper corners and new materials with greater expansion coefficients.[39]

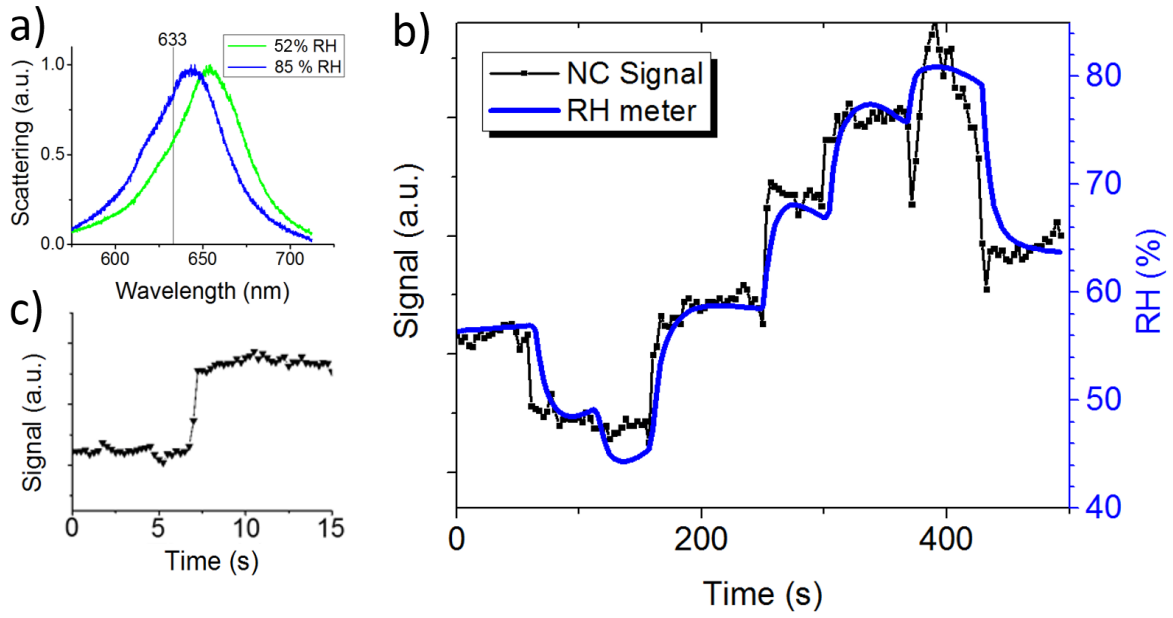

Figure 5. (a) White-light scattering spectra of NC peaks under changing humidity conditions showing the position of the laser wavelength. (b) Scattering intensity of a single NC above a 11 nm spacer illuminated by TM polarized 633 nm laser emission as RH is varied, compared to the readings from a commercial electrochemical sensor. Plot (c) highlights the fast response time of the NC system for a measured RH change of 50-67%.

Another approach to measuring RH change is to illuminate the sample with monochromatic light with a resonance chosen so that under ambient conditions the illumination wavelength falls approximately half way up the scattering peak (**figure 5**(a)). Using monochromatic light allows for faster and more precise observation of a signal change, and is a more scalable method as it does not require a bulky and expensive spectrometer to measure shifts.

FDTD simulations show that the scattering spectrum of a 75 nm, 10 nm RoC NC, is well approximated by a straight line (with an R^2 coefficient of determination of 0.989) within 75 % the spectral distance from the FWHM to the peak, meaning that careful tuning of the NC resonance is required for monochromatic sensing. Data from this approach can be seen in figure 5(b), where a 633 nm red laser was used to illuminate an individual NC. In this plot, an NC with an ambient peak of 653 nm was illuminated and the RH varied between 45-80%. The measured intensity of the NC scattering is well matched to the RH shifts recorded using a commercial electrochemical sensor, except for at an RH of 45 % where the response of the Nafion film to RH ceases to be linear, and an inferior response is to be expected in this region. This results justifies the assumptions of linearity made in this chapter. Through examining the change in photon count in the single-photon avalanche diode (SPAD) with RH shift, this approach was found to produce a RH sensitivity of 0.09 dB/% RH, which again is a marked improvement on previous single NP humidity sensors.[6] The r.m.s. variance of the signal

measured at a constant humidity gives a noise-limited resolution for the sensor of 0.9 % RH, although this is dependent on the assumptions of linearity of both the film expansion and the slope of the NC scattering peak.

The initial response of the sensor to a change in humidity is extremely rapid, figure 5(c) shows a step with an RH shift of 17 % and the response here for 90% of the signal change occurs across ~200 ms, although this could be limited by the rate moist air is injected into the system and the actual maximum could be significantly higher. Nafion is known to have a quick response time to humidity change, Santos *et al* found a response of 242 ms for a 3% RH variation with 35 μm films,[33] and so this is not surprising, especially as these films are only 10-20 nm thick and the hydrophilic domain size is estimated to be 1-3 nm,[40] so there are very few layers of molecules that the water must diffuse through before it has completely permeated the polymer.

We now compare these results with other sensors in the field. The most common type of humidity sensor is an electrochemical design with a water-reactive film placed between two electrodes, have shown high sensitivities, with impedance changes of several orders of magnitude with RH[41–45] and response times usually around several seconds.[46,47] The most common optical sensors take the form of optical fibers coated with a reactive material which changes the confinement of the mode in response to RH.[33,47–5051] These designs have response times ranging from 10 ms[48] – 0.5 minutes[49] and have resolutions up to 0.01%RH across a broad range.[3347]

In recent years there has been a concerted drive to produce sensing elements that can be integrated with nano and micro scale optical circuitry, to comply with lab-on-a-chip devices and other emerging technologies. Gas sensors have been constructed based upon whispering gallery resonators,[52] gas sensitive photonic crystals,[53] nanowires above sensitive polymer

films,[54,55] specially fabricated nanoparticles[7,38] and nanoparticles embedded in polymer optical nanofibers.[6] Nanoscale humidity sensors typically achieve resolutions between 0.1 – 1 %RH, and response times on the order of 100 ms.[6,52,54] The patch antenna geometry presented here performs well compared to other nanoscale designs, and better than existing single particle models.[6,38] It has the additional benefit of significantly easier fabrication, requiring no complex apparatus or top-down processing, and the possibility for ready integration with various waveguide designs.

We have demonstrated that thinner spacers produce more sensitive detectors, due to the approximately reciprocal relationship between thickness and the effective refractive index of the mode. It is also possible to tune the resonance and the sensitivity by changing the size and shape of the nanocubes, which is investigated using FDTD simulations.

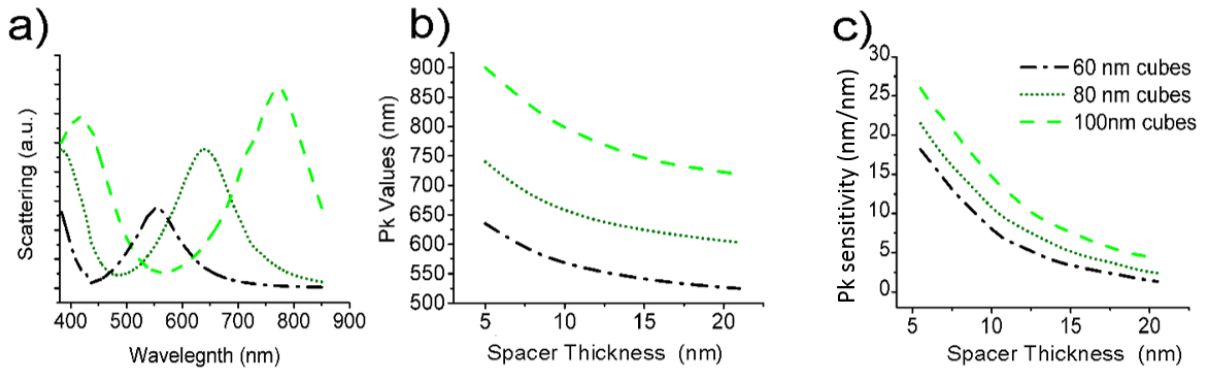

Figure 6. (a) FDTD simulation of the scattering spectra of 75 nm Ag NC's with 10 nm RoC above a 12 nm film with a 2 nm PVP layer as the cube width is varied from 60-100 nm. (b) Plotting the resonance peaks of the NC's for spacer thicknesses from 5-22 nm. (c) Plotting the sensitivities of the peak position to a 1 nm increase in spacer thickness for 60-100 nm NC's.

Figure 6(a) illustrates the effect of cube size on the scattering spectra of NC's with 10 nm corners above a spacer of 12 nm, while 6(b) shows that the cube size is more significant in tuning the resonance wavelength than spacer thickness for the parameter range under consideration. An increase in sensitivity for larger NC's is seen in figure 6(c), but reducing the film thickness is seen to be a much more significant factor in this range. For cubes above a 5 nm spacer, where the values for varying cube size are the most divergent, the sensitivity only changes by ~8 nm/nm for a 40 nm change in size, whereas by changing spacer thickness from 5 to 20 nm, the sensitivity varies between 2 – 22 nm/nm.

This behaviour fits well with our understanding of the patch antenna model. We have stated that the resonance wavelength is dependent on both NC size and spacer thickness: $\lambda_{pk} \sim w$ and, loosely $\lambda_{pk} \sim 1/t$. The sensitivity of the peak to a change in spacer thickness, $S_t = d\lambda_{pk}/dt$ comes down to a derivative of the expression in eq. S2 and will therefore be extremely sensitive to thickness changes in thin films, whilst the size dependence remains linear. For tuning λ_{pk}, the greater range of sizes accessible for NC fabrication make it the more useful parameter.

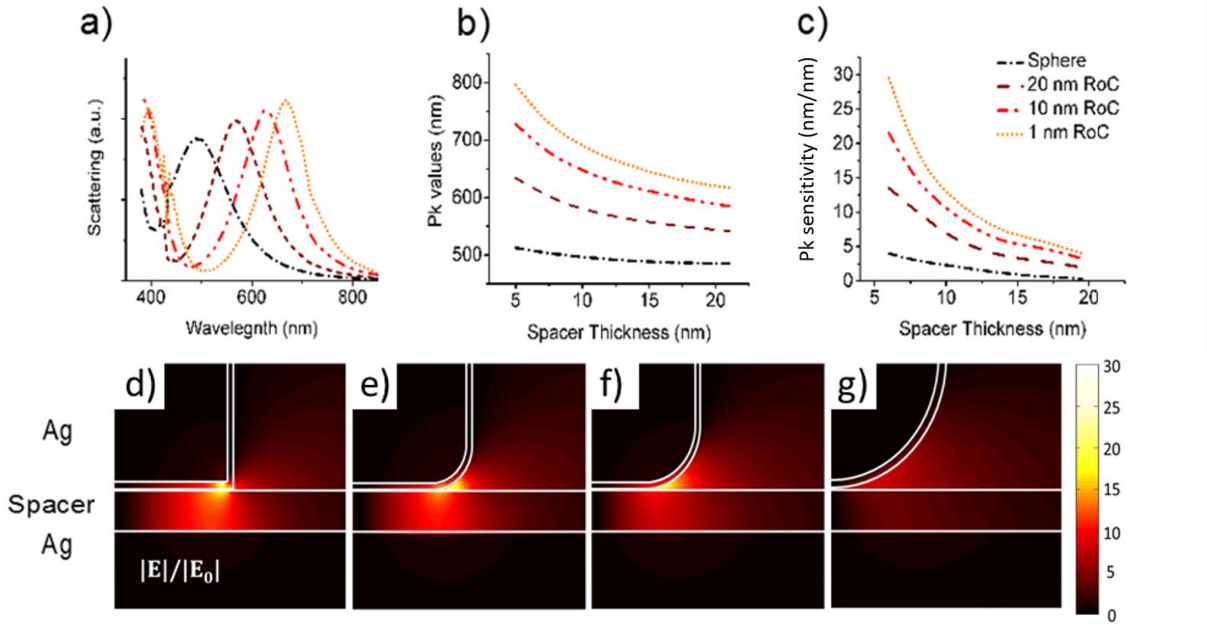

Figure 7. (a) FDTD simulation of the scattering spectra of 75 nm Ag NC's above a 12 nm film with a 2 nm PVP layer as the RoC of the corners is varied from 1-37.5 nm at which point the NC becomes a sphere. (b) Plotting the resonance peaks of the NC's for spacer thicknesses from 5-21 nm. (c) Plotting the sensitivities of the peak position to a 1 nm increase in spacer thickness. (d-g) Electric field intensity plots showing the mode geometry about the corners as the RoC increases from 1 nm (d) to 37.5 nm (g).

The effect corner radius of curvature has on the modes is more complex: Reducing the RoC produces both a pronounced redshift of the peak and a significant increase in the sensitivity. This behaviour is displayed in **figure 7**(a-c) for 75 nm NC's with a RoC from 1 nm to 37.5 nm (a spherical particle). Examining the electric field intensity of the modes in figure 7(d-g), the points of greatest field strength in the film are separated by 73 nm for a NC with 1 nm corners, but only 53 nm for a cube with 20 nm RoC corners. It can be seen that the mode maxima is located close to the start of the corner curve, so even the slightest beveling appears to have a significant effect on the plasmon resonance. Bowen and Smith[25] found that defining an effective width for NC's with rounded corners was necessary to accurately model the scattering behaviour. We postulate that reduced λ_{pk} values for more rounded corners are due to scattering of the free electrons that make up the surface plasmons at the start of the curved edges. This reduces the effective size of the plasmonic cavity, which leads to resonances at shorter wavelengths than would be expected for a given size of cube.

As well as scattering of the free electrons, the addition of the corners also promotes the formation of gap modes between the NC and the spacer. Here the evanescent field becomes highly concentrated in the small gap due to its low refractive index,[56] at the cost of the mode in the film, and the simulations show that for any corner rounding at all, the strongest field concentration is in this gap. In figure 7(d-g), as the RoC is increased a clear reduction of the electric field strength in the spacer can be observed, meaning that the resonance conditions of

this system will become less sensitive to what is happening in the film as RoC is increased, which is highly undesirable for a sensor which depends on the film response. For a doubling of the corner RoC from 10-20 nm for 75 nm NC's above a 13 nm film, a ~40% decrease in the sensitivity is predicted.

This modelling suggests that the sensitivity of our device can be greatly enhanced. For a 100 nm NC, with 5 nm corners above a 5 nm Nafion film, parameters which have been shown to be achievable,[57,58] a peak sensitivity to thickness change of around 43 nm/nm is expected, which translates to a humidity sensitivity of 1.3 nm/% RH, over three times better than the best average from this investigation, and more than double the best individual result.

As well as further enhancements to the sensitivity, future work should focus on the integration of this sensor with plasmonic circuitry. If a single NC was deposited above a metal waveguide with a <10 nm Nafion spacer, the humidity response of the system would result in a difference in the attenuation of a surface plasmon polariton sent down the waveguide. Due to the extremely concentrated modes excited between the cube and the metal substrate we anticipate that this would be significantly more sensitive than detectors using a strip waveguide coated with solely a reactive polymer layer. This is supported by the work of Mock *et al*, who demonstrated that the modes excited between spheres and a metal films are more sensitive to spacer thickness than the surface plasmon polaritons excited in the metal film using a prism.[59] Thus this system has the potential to operate as a fully integrated component in a plasmonic circuit, opening the way to a new class of on-chip nanoscale sensors.

A further benefit of this design is that it can be utilised to detect any number of chemicals as long as appropriate spacer materials can be found. There are many polymers which expand in response to a specific chemical, or class of chemicals, which would allow for the detection of

analytes as diverse as alcohols, using poly(methyl methacrylate) as the spacer,[53] to nitroaromatic explosives such as TNT using poly(4-vinylpyridine).[60]

To conclude, in this report we have demonstrated the operation of the nanopatch antenna system as a novel, sub-wavelength optical humidity sensor and explored the limits of its sensitivity. We have shown that by using Nafion, a polymer which expands with increasing humidity, as the spacer layer between a silver nanocube and silver sheet we can produce a nanoscale sensor with a fast response time and higher sensitivity than any other single-particle plasmonic humidity sensor recorded. Sensitivities up to 0.57 nm/% RH are recorded, and a resolution of better than 1 % RH achieved. FDTD models predict that the sensitivity can be more than doubled from the recorded maximum through careful choice of structural parameters. An appropriate choice of alternative spacer materials would enable this structure to detect a variety of other gases. This system is easy to fabricate and is an extremely scalable design - arrays of NC's could be created to form a large-scale metamaterial, or kept as a single-NC system with a sub-wavelength footprint and the potential to be integrated into photonic circuitry.

Experimental Section

Silver Nanocubes were purchased from Nanocomposix and characterised using a Jeol 3000F TEM. They were found to have an average length of 75 ± 4 nm, with a corner radius of curvature (RoC) of 10 ± 2 nm (figure S2), with a PVP buffer layer of around 2-3 nm. These were diluted in deionized water at a ratio of 1:50 and sonicated before use.

Wafers of silicon were cleaned in acetone and isopropanol, then either coated with 100 nm of Ag in an evaporation chamber or left bare for ellipsometry measurements. Nafion was

bought as a resin from Sigma-Aldrich and diluted in ethanol to 0.5 or 0.25% wt. The Nafion was then dropped onto the sample through a 0.2 μm PVDF filter and spincast for 60s at speeds of 1000-4000 rpm. Samples were heated to 70 ^{o}C under vacuum for 2 hours to promote adhesion of the Nafion to the substrate. Ellipsometry was performed on Nafion films spin-coated onto Si substrates under controlled humidity conditions using a J.A. Woollam, Alpha-SE ellipsometer.

The NC's were adsorbed onto the Nafion layer using the method described by Moreau et al.[20] In brief – after sonication, 30 μL of NC solution was dropped onto a cleaned coverslip and the sample was placed on top. The nanocubes adsorb to the surface and most aggregations drop away. The surface density is determined by the time in contact with the solution.

The samples were then placed in a sealed chamber containing an electrochemical humidity sensor from Thorlabs (TSP01) with two pipes connected to dry and moist air chambers and a pressure release valve to control the relative humidity around the sample. The humidity chamber was then connected to a dark-field microscope with TM polarised illumination either from a white light source or 632 nm red laser, focused onto the sample at an angle of 60^{o} from the normal so that all specular reflection not interacting with the NC's would not be collected by the long (22 mm) focal length 0.8 NA objective. When using the laser an APD was used to confirm the stability of the red laser before interaction with the sample. After the objective a beam splitter directs some light to a CCD for imaging. Two telecentric lenses focus light through a 50 μm pinhole aperture to allow for single NC selection. Light from the selected cube was then directed into a SPAD and an Andor spectrograph.

Simulated results were achieved using the Lumerical finite-difference time-domain (FDTD) simulation package. Nafion is simulated as a dielectric with a thickness-dependent refractive index taken from the ellipsometry data shown in figure S4. PVP is simulated as a dielectric

with an RI of 1.5. All simulations were conducted in 2D to conserve processing time. It has been previously shown that the underlying physics between a nanocube and a nanostrip in this structure are very close,[20,36] and that the orientation of the NC does not affect the resonance frequency of a cube.[21,22,61] This has been confirmed by contrasting selected 2D and 3D simulations.

Supporting Information
Supporting Information is available from the Wiley Online Library or from the author.

Acknowledgements
AWP acknowledges support from the UK Engineering and Physical Sciences Research Council.

Received: ((will be filled in by the editorial staff))
Revised: ((will be filled in by the editorial staff))
Published online: ((will be filled in by the editorial staff))

1. Cao, J., Galbraith, E. K., Sun, T. & Grattan, K. T. V. Cross-Comparison of Surface Plasmon Resonance-Based Optical Fiber Sensors With Different Coating Structures. *Sensors Journal, IEEE* **12**, 2355–2361 (2012).
2. Mayer, K. M. & Hafner, J. H. Localized Surface Plasmon Resonance Sensors. *Chemical Reviews* **111**, 3828–3857 (2011).
3. Zamborini, F. P., Bao, L. & Dasari, R. Nanoparticles in Measurement Science. *Analytical Chemistry* **84**, 541–576 (2012).
4. Haynes, C. L., McFarland, A. D. & Duyne, R. P. V. Surface-enhanced Raman spectroscopy. *Analytical Chemistry* **77**, 338–A (2005).
5. Jung, S.-A. *et al.* Thickness dependence of surface plasmon resonance sensor response for metal ion detection. *Journal of Physics D: Applied Physics* **46**, 315104 (2013).
6. Wang, P. *et al.* Polymer Nanofibers Embedded with Aligned Gold Nanorods: A New Platform for Plasmonic Studies and Optical Sensing. *Nano Letters* **12**, 3145–3150 (2012).
7. Liu, N., Tang, M. L., Hentschel, M., Giessen, H. & Alivisatos, A. P. Nanoantenna-enhanced gas sensing in a single tailored nanofocus. *Nature materials* **10**, 631–636 (2011).
8. Ma, R.-M., Ota, S., Li, Y., Yang, S. & Zhang, X. Explosives detection in a lasing plasmon nanocavity. *Nature nanotechnology* **9**, 600–604 (2014).
9. Roh, S., Chung, T. & Lee, B. Overview of the characteristics of micro-and nano-structured surface plasmon resonance sensors. *Sensors* **11**, 1565–1588 (2011).

10. Sorger, V. J., Oulton, R. F., Ma, R.-M. & Zhang, X. Toward integrated plasmonic circuits. *MRS bulletin* **37**, 728–738 (2012).
11. Day, J. K., Neumann, O., Grady, N. K. & Halas, N. J. Nanostructure-Mediated Launching and Detection of 2D Surface Plasmons. *ACS Nano* **4**, 7566–7572 (2010).
12. Chen, H., Kou, X., Yang, Z., Ni, W. & Wang, J. Shape- and Size-Dependent Refractive Index Sensitivity of Gold Nanoparticles. *Langmuir* **24**, 5233–5237 (2008).
13. Cheng, Y., Wang, M., Borghs, G. & Chen, H. Gold nanoparticle dimers for plasmon sensing. *Langmuir* **27**, 7884–7891 (2011).
14. Chung, T., Lee, S.-Y., Song, E. Y., Chun, H. & Lee, B. Plasmonic nanostructures for nano-scale bio-sensing. *Sensors* **11**, 10907–10929 (2011).
15. Lee, K. & Irudayaraj, J. Correct spectral conversion between surface-enhanced Raman and plasmon resonance scattering from nanoparticle dimers for single-molecule detection. *small* **9**, 1106–1115 (2013).
16. Anker, J. N. *et al.* Biosensing with plasmonic nanosensors. *Nature Materials* **7**, 422 (2008).
17. Hill, R. T., Kozek, K. M., Hucknall, A., Smith, D. R. & Chilkoti, A. Nanoparticle-Film Plasmon Ruler Interrogated with Transmission Visible Spectroscopy. *ACS Photonics* **1**, 974–984 (2014).
18. Hill, R. T. *et al.* Plasmon Ruler with Angstrom Length Resolution. *ACS Nano* **6**, 9237–9246 (2012).
19. Henzie, J., Andrews, S. C., Ling, X. Y., Li, Z. & Yang, P. Oriented assembly of polyhedral plasmonic nanoparticle clusters. *Proceedings of the National Academy of Sciences* **110**, 6640–6645 (2013).
20. Edwards, A. P. & Adawi, A. M. Plasmonic nanogaps for broadband and large spontaneous emission rate enhancement. *Journal of Applied Physics* **115**, (2014).
21. Lassiter, J. B. *et al.* Plasmonic Waveguide Modes of Film-Coupled Metallic Nanocubes. *Nano Letters* **13**, 5866–5872 (2013).
22. Moreau, A. *et al.* Controlled-reflectance surfaces with film-coupled colloidal nanoantennas. *Nature* **492**, 86–89 (2012).
23. Akselrod, G. M. *et al.* Probing the mechanisms of large Purcell enhancement in plasmonic nanoantennas. *Nature Photonics* (2014).at <http://www.nature.com/nphoton/journal/v8/n11/full/nphoton.2014.228.html>
24. Rose, A. *et al.* Control of Radiative Processes Using Tunable Plasmonic Nanopatch Antennas. *Nano Letters* **14**, 4797–4802 (2014).
25. Bowen, P. T. & Smith, D. R. Coupled-mode theory for film-coupled plasmonic nanocubes. *Phys. Rev. B* **90**, 195402 (2014).
26. Cirací, C., Britt Lassiter, J., Moreau, A. & Smith, D. R. Quasi-analytic study of scattering from optical plasmonic patch antennas. *Journal of Applied Physics* **114**, (2013).
27. Dishari, S. K. & Hickner, M. A. Antiplasticization and Water Uptake of Nafion Thin Films. *ACS Macro Letters* **1**, 291–295 (2012).
28. Dura, J. A., Murthi, V. S., Hartman, M., Satija, S. K. & Majkrzak, C. F. Multilamellar interface structures in Nafion. *Macromolecules* **42**, 4769–4774 (2009).
29. Ogata, Y., Kawaguchi, D., Yamada, N. L. & Tanaka, K. Multistep Thickening of Nafion Thin Films in Water. *ACS Macro Letters* **2**, 856–859 (2013).
30. Bozhevolnyi, S. I. & Søndergaard, T. General properties of slow-plasmon resonant nanostructures: nano-antennas and resonators. *Opt. Express* **15**, 10869–10877 (2007).
31. Kurokawa, Y. & Miyazaki, H. T. Metal-insulator-metal plasmon nanocavities: Analysis of optical properties. *Phys. Rev. B* **75**, 035411 (2007).

32. Wu, C. *et al.* Large-area wide-angle spectrally selective plasmonic absorber. *Phys. Rev. B* **84**, 075102 (2011).
33. Santos, J. S. *et al.* Characterisation of a Nafion film by optical fibre Fabry–Perot interferometry for humidity sensing. *Sensors and Actuators B: Chemical* **196**, 99–105 (2014).
34. Petrina, S. A. Water sorption, visoelastic, and optical properties of thin Nafion films. (2013).
35. Modestino, M. A. *et al.* Self-Assembly and Transport Limitations in Confined Nafion Films. *Macromolecules* **46**, 867–873 (2013).
36. Tang, Y. *et al.* An experimental investigation of humidity and temperature effects on the mechanical properties of perfluorosulfonic acid membrane. *Materials Science and Engineering: A* **425**, 297–304 (2006).
37. Aleksandrova, E. *et al.* Proton conductivity study of a fuel cell membrane with nanoscale resolution. *ChemPhysChem* **8**, 519–522 (2007).
38. Bingham, J. M., Anker, J. N., Kreno, L. E. & Van Duyne, R. P. Gas sensing with high-resolution localized surface plasmon resonance spectroscopy. *Journal of the American Chemical Society* **132**, 17358–17359 (2010).
39. Si, K., Dong, D., Wycisk, R. & Litt, M. Synthesis and characterization of poly (para-phenylene disulfonic acid), its copolymers and their n-alkylbenzene grafts as proton exchange membranes: high conductivity at low relative humidity. *Journal of Materials Chemistry* **22**, 20907–20917 (2012).
40. Malek, K. *et al.* Nanophase segregation and water dynamics in hydrated Nafion: Molecular modeling and experimental validation. *The Journal of Chemical Physics* **129**, (2008).
41. Lv, X., Li, Y., Li, P. & Yang, M. A resistive-type humidity sensor based on crosslinked polyelectrolyte prepared by {UV} irradiation. *Sensors and Actuators B: Chemical* **135**, 581–586 (2009).
42. Su, M., Wang, J. & Hao, Y. Development of Y 3+ and Mg 2+-doped zirconia thick film humidity sensors. *Materials Chemistry and Physics* **126**, 31–35 (2011).
43. Wang, W. *et al.* Humidity sensor based on LiCl-doped ZnO electrospun nanofibers. *Sensors and Actuators B: Chemical* **141**, 404–409 (2009).
44. Wu, R.-J., Sun, Y.-L., Lin, C.-C., Chen, H.-W. & Chavali, M. Composite of TiO2 nanowires and Nafion as humidity sensor material. *Sensors and Actuators B: Chemical* **115**, 198–204 (2006).
45. Zhang, Y. *et al.* A novel humidity sensor based on NaTaO3 nanocrystalline. *Sensors and Actuators B: Chemical* **174**, 485–489 (2012).
46. Farahani, H., Wagiran, R. & Hamidon, M. N. Humidity Sensors Principle, Mechanism, and Fabrication Technologies: A Comprehensive Review. *Sensors* **14**, 7881 (2014).
47. Tripathy, A., Pramanik, S., Cho, J., Santhosh, J. & Abu Osman, N. A. Role of Morphological Structure, Doping, and Coating of Different Materials in the Sensing Characteristics of Humidity Sensors. *Sensors* **14**, 16343–16422 (2014).
48. Aneesh, R. & Khijwania, S. K. Titanium dioxide nanoparticle based optical fiber humidity sensor with linear response and enhanced sensitivity. *Appl. Opt.* **51**, 2164–2171 (2012).
49. Shukla, S., Tiwari, A., Parashar, G., Mishra, A. & Dubey, G. Exploring fiber optic approach to sense humid environment over nano-crystalline zinc oxide film. *Talanta* **80**, 565—571 (2009).

50. Yeo, T. L. *et al.* Characterisation of a polymer-coated fibre Bragg grating sensor for relative humidity sensing. *Sensors and Actuators B: Chemical* **110**, 148–156 (2005).
51. Urrutia, A., Goicoechea, J., Rivero, P. J., Matías, I. R. & Arregui, F. J. Electrospun nanofiber mats for evanescent optical fiber sensors. *Sensors and Actuators B: Chemical* **176**, 569–576 (2013).
52. Mehrabani, S., Kwong, P., Gupta, M. & Armani, A. M. Hybrid microcavity humidity sensor. *Applied Physics Letters* **102**, (2013).
53. Clevenson, H., Desjardins, P., Gan, X. & Englund, D. High sensitivity gas sensor based on high-Q suspended polymer photonic crystal nanocavity. *Applied Physics Letters* **104**, (2014).
54. Gu, F., Zeng, H., Tong, L. & Zhuang, S. Metal single-nanowire plasmonic sensors. *Opt. Lett.* **38**, 1826–1828 (2013).
55. Gu, F., Zhang, L., Yin, X. & Tong, L. Polymer Single-Nanowire Optical Sensors. *Nano Letters* **8**, 2757–2761 (2008).
56. Green, M. A. Enhanced evanescent mode light trapping in organic solar cells and other low index optoelectronic devices. *Progress in Photovoltaics: Research and Applications* **19**, 473–477 (2011).
57. DeCaluwe, S. C., Kienzle, P. A., Bhargava, P., Baker, A. M. & Dura, J. A. Phase segregation of sulfonate groups in Nafion interface lamellae, quantified via neutron reflectometry fitting techniques for multi-layered structures. *Soft matter* **10**, 5763–5776 (2014).
58. Martinsson, E., Otte, M. A., Shahjamali, M. M., Sepulveda, B. & Aili, D. Substrate Effect on the Refractive Index Sensitivity of Silver Nanoparticles. *The Journal of Physical Chemistry C* **118**, 24680–24687 (2014).
59. Mock, J. J. *et al.* Distance-Dependent Plasmon Resonant Coupling between a Gold Nanoparticle and Gold Film. *Nano Letters* **8**, 2245–2252 (2008).
60. Tenhaeff, W. E., McIntosh, L. D. & Gleason, K. K. Synthesis of Poly(4-vinylpyridine) Thin Films by Initiated Chemical Vapor Deposition (iCVD) for Selective Nanotrench-Based Sensing of Nitroaromatics. *Advanced Functional Materials* **20**, 1144–1151 (2010).
61. Zhao, H., Yang, Y., Li, Q. & Qiu, M. Sub-wavelength quarter-wave plate based on plasmonic patch antennas. *Applied Physics Letters* **103**, (2013).

Submitted to ADVANCED OPTICAL MATERIALS

A humidity sensor based on the plasmonic response of a nanocube and metal surface separated by a polymer with high expansion coefficient when exposed to water. The sensing element has a sub-wavelength footprint and exhibits a high sensitivity and fast reaction times compared to other plasmonic sensors. The sensitivity dependence on both nanocube and polymer layer parameters is theoretically investigated.

Keywords: gas; humidity; nanocube; plasmon; sensor; waveguide

Alexander W. Powell, David M. Coles, Robert A. Taylor, Andrew A.R. Watt, Hazel E. Assender and Jason M. Smith*

Plasmonic Gas Sensing using Nanocube Patch Antennas

ToC figure